Biocatalysis

DOI: 10.1002/ange.201304633

Inversion of Enantioselectivity of a Mononuclear Non-Heme Iron(II)-dependent Hydroxylase by Tuning the Interplay of Metal-Center Geometry and Protein Structure**

*Sarah M. Pratter, Cornelia Konstantinovics, Cristiana M. L. Di Giuro, Erich Leitner, Devesh Kumar, Sam P. de Visser, Gideon Grogan, and Grit D. Straganz**

Natural stereoselective oxidations by molecular oxygen have long fascinated chemists and these chemically challenging, "green" reactions have great potential for industrial processes.[1] However, the natural enzymes have a finite synthetic repertoire. A major goal is therefore to control their stereoselectivity and to produce a desired stereo-center within a certain target molecule. There have been some major successes recently in the design of stereo-controlled reactions by cytochrome P450 enzymes (P450s),[2] which have great potential as a source for site-specific oxygenation reactions.[3] By contrast, O_2 and mononuclear non-heme (MNH) Fe^{II} dependent hydroxylases have not been the focus of enzyme design studies. This is surprising because the catalytic potential of MNH Fe^{II} dependent hydroxylases complements that of P450s, with their ability to oxidize aliphatic carbon atoms in a regio- and stereoselective manner.[4] One example is the (*S*)-selective *p*-hydroxymandelate synthase (HMS) from *Amycalotopsis orientalis* (*Ao*HMS), which has homologues in other organisms including *Streptomyces coelicolor* (*Sc*HMS).[5,6] Recently, it was found that the high enantioselectivity of *Sc*HMS, which naturally converts the substrate *p*-hydroxyphenylpyruvate, can be compromised by substituents on the aromatic ring of phenylpyruvate (PP).[7] However, no structural features have been identified that cause the generally observed (*S*)-enantioselectivity of HMS enzymes. Herein, we have used modeling, molecular dynamics (MD), and density functional theory (DFT) calculations to redesign the (*S*)-selective *Sc*HMS to give a biocatalyst of inverted enantioselectivity, yielding (*R*)-mandelate as the product.

The reaction mechanism of HMS enzymes follows that of α-ketoacid dependent MNH Fe^{II} enzymes: *p*-hydroxyphenylpyruvate binding primes the iron center for activation of O_2, which in turn decarboxylates the substrate. The resulting high-valent Fe^{IV}=O species abstracts a benzylic hydrogen atom. In a rebound reaction, the formed Fe^{III}–OH species transfers a hydroxyl radical to the benzylic position resulting in the *p*-hydroxymandelate product, which leaves the active site (Figure 1).[6,8] The crystal structure of the (*S*)-selective *Ao*HMS has been determined and shows the native reaction product coordinated to the metal center.[9]

Upon close inspection of in silico docked complexes of *Sc*HMS with mandelate (MA) analogues of the (*S*)-configuration, as well as in the *Ao*HMS crystal structure,[9] it was found that the ligands were oriented in a slightly distorted trigonal bipyramidal geometry at the metal center. The α-hydroxy group of MA and the metal-coordinating glutamate were in the axial positions and two nitrogen atoms from the coordinating histidines, together with the carboxylate oxygen of the ligand, formed the trigonal basis of the pyramid. In contrast, the analogous (*R*)-MA–enzyme complex showed more pronounced deviations from the ideal symmetry (Supporting Information, Figure S1).[7] DFT calculations of the reactive Fe^{IV}=O and Fe^{III}–OH species in the catalytic cycle of α-ketoacid dependent enzymes showed that a trigonal bipyramidal geometry was one of two probable organizations

[*] S. M. Pratter, C. Konstantinovics, Dr. C. M. L. Di Giuro, Dr. G. D. Straganz
Institute of Biotechnology and Biochemical Engineering
Graz University of Technology
Petersgasse 12, 8010 Graz (Austria)
E-mail: grit.straganz@tugraz.at
Prof. Dr. E. Leitner
Institute of Analytical Chemistry and Food Chemistry
Graz University of Technology
Stremayrgasse 9, 8010 Graz (Austria)
Dr. D. Kumar
Department of Applied Physics, School for Physical Sciences,
Babasaheb Bhimrao Ambedkar University
Vidya Vihar, Rae Bareilly Road, Lucknow 226-025 (India)
Dr. S. P. de Visser
Manchester Institute of Biotechnology and School of Chemical Engineering and Analytical Science
The University of Manchester
131 Princess Street, Manchester M1 7DN (UK)
Dr. G. Grogan
York Structural Biology Laboratory, Department of Chemistry,
University of York
Heslington, York, YO10 5DD (UK)

[**] The financial support by the Austrian Science Fund (FWF) grant W901-B05 DK Molecular Enzymology and FWF research grant P18828 is gratefully acknowledged. G.D.S. thanks the VVRC at the Graz University of Technology for computational resources and Kim Carstens for technical assistance. S.d.V. thanks the National Service of Computational Chemistry Software for CPU time. D.K. holds a Ramanujan Fellowship from the Department of Science and Technology (DST), New Delhi (India) and acknowledges its financial support (Research Grants SR/S2/RJN-11/2008 and SR/S1/PC-58/2009).

Supporting information for this article is available on the WWW under http://dx.doi.org/10.1002/anie.201304633.

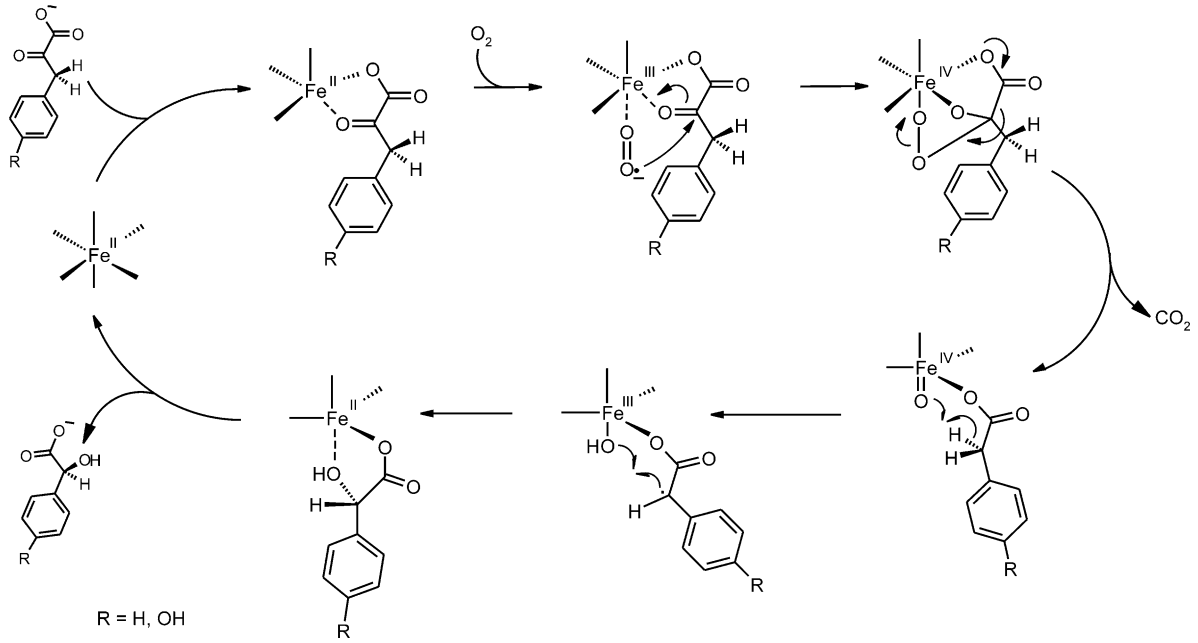

Figure 1. Generally accepted reaction mechanism of HMS enzymes.[8]

of these high-valent iron centers.[10] This posed the question of what impact the ligand field symmetry may have on enantioselectivity during catalysis. In models of (*R*)-MA and (*S*)-MA bound *Sc*HMS, in which the trigonal bipyramidal geometry was constrained, the (*R*)-MA ligand did not occupy the hydrophobic pocket that accommodates the aromatic substituent of (*S*)-MA. In contrast, the aromatic ring pointed toward the presumed substrate entrance channel and thereby collided with residue Tyr359 (Figure S1). *pro*-(*S*) and *pro*-(*R*) transition states of H-abstraction and rebound hydroxylation gave analogous principle spatial orientations when docked into the trigonal bipyramidal metal center of *Sc*HMS. Consequently, we investigated how the destabilization of the aromatic ring in the hydrophobic pocket and its stabilization in the alternative orientation influenced enantioselective catalysis. The steric clash with residue Tyr359 upon (*R*)-MA binding in our model could be removed by substituting it with alanine. To obstruct the hydrophobic pocket of *Sc*HMS, potentially effective point mutations were identified using in silico site-saturation mutagenesis with the following set of criteria: the variation 1) results in a low-energy apo-enzyme structure to prevent energetically driven reorganization of the active site; 2) has low-energy amino acid conformers that all interfere with the hydrophobic binding pocket; and 3) does not interact with the first coordination sphere of the metal ion and thus with its electronic or geometric structure. Using the algorithm described in the Supporting Information (Figure S2), six target single-point substitutions (Ser221Met, Val223Phe, Val223Met, Val223Trp, Ile236Phe and Tyr359Ala) were identified and introduced into the *Sc*HMS scaffold in vitro.

Spectra of PP conversion products by the wild-type (WT) and the resulting enzyme variants were subsequently analyzed using GC-MS and HPLC-MS (Table S1): all but one variation had a significant impact on the enantioselectivity of the WT enzyme, which gave an enantiomeric ratio (e.r.) of 0.4% (*R*)-MA:99.6% (*S*)-MA (Figure 2a). The most pronounced effect was an appoximately 1900-fold increase in (*R*)-selectivity with the mutation Ser221Met, which was predicted to obstruct the hydrophobic pocket, and resulted in the formation of 88.5% (*R*)-MA versus 11.5% (*S*)-MA. This efficacy was followed by the mutant Val223Phe, which gave an e.r. of 65.1% (*R*)-MA:34.9% (*S*)-MA. The opening of space for (*R*)-MA binding by the Tyr359Ala mutation resulted in only an approximately 47-fold increase of (*R*)-enantioselectivity compared to WT. Notably, Ser221, Val223, and Tyr359 are strongly conserved throughout all annotated putative *p*-hydroxyphenylpyruvate dioxygenases and HMSs. Combinations of the most successful substitutions further enhanced enantioselectivity: the best variant, triple mutant Ser221Met_Val223Phe_Tyr359Ala increased the e.r. to 97.4% in favor of (*R*)-selective hydroxylation, which corresponds to an approximately 9300-fold enhancement compared to WT. The latter translates to a difference in transition state energy $\Delta\Delta G^{\ddagger}$ of 22.6 kJ mol^{-1}. No reaction side products that are indicative of C2–C3 cleavage or uncoupled decarboxylation[11] were formed in detectable amounts and product recovery for MA was greater than 95% for all variants, except for variants Ile236Phe and Val223Trp, which showed substantial losses of approximately 60% and 20% that were not accounted for. This may indicate the formation of alternative oxygenation products in these variants that escaped our analysis. Notably, ring oxidation products have been reported from mutational studies of the active site of HMS.[12]

All *Sc*HMS variants had enzymatic activities towards PP that were roughly in the same range of the WT enzyme (Figure 2b, Table S1). The point mutations Val223Phe and Ser221Met increased catalytic efficiencies by an order of

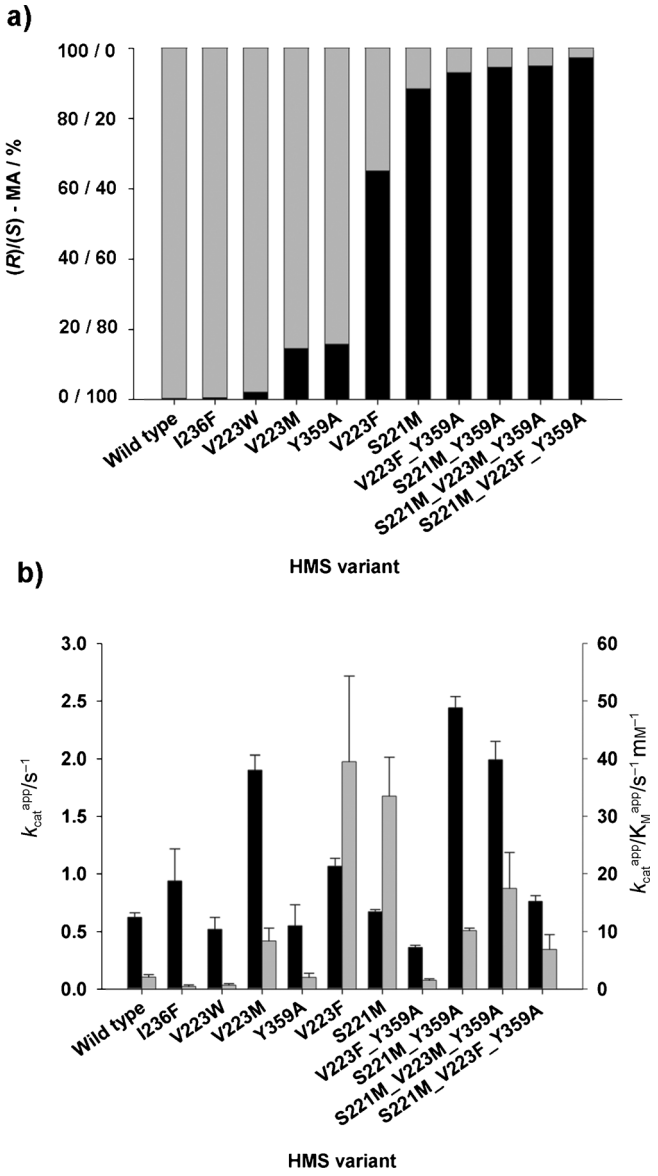

Figure 2. Enantioselectivities and activities of *Sc*HMS WT and variants. (a) The percentage of (*R*)-MA (black) and (*S*)-MA (gray) products and (b) steady-state kinetic constants k_{cat}^{app} (black) and k_{cat}^{app}/K_M^{app} (gray) are shown.

magnitude with k_{cat}^{app}/K_M^{app} values of 40 mM^{-1}s^{-1} and 34 mM^{-1}s^{-1} respectively, while the open active-site variant Tyr359Ala did not significantly alter WT efficiency ($k_{cat}^{app}/K_M^{app} = 2.1$ mM^{-1}s^{-1}). For the enzyme with the highest (*R*)-enantioselectivity, the triple mutant Ser221Met_Val223Phe_Tyr359Ala, the apparent turnover number was raised by 22% ($k_{cat}^{app} = 0.76$ s^{-1}) and the k_{cat}^{app}/K_M^{app} of 6.9 mM^{-1}s^{-1} was approximately three times higher compared to the WT enzyme.

The structure of the newly designed (*R*)-MA synthase, *Sc*HMS variant Ser221Met_Val223Phe_Tyr359Ala, in complex with (*R*)-MA and cobalt, which is a redox inactive Fe^{II} mimic,[9] was solved and refined to a resolution of 1.95 Å with an R_{cryst} value of 17.5% and an R_{free} value of 21.5% (Table S2). The aromatic substituent of the product filled the free space, which was created by the Tyr359Ala mutation, while Met221 and Phe223 occupied space in the hydrophobic binding pocket of the enzyme. Both protein molecules of the asymmetric unit showed (*R*)-MA ligation to the metal ions in a trigonal bipyramidal geometry and thus mirrored the product coordinated active site in the native structure of *Ao*HMS[11] (Figure 3a).

Computational MD studies of reaction intermediates in the scaffolds of WT *Sc*HMS and its Ser221Met_Val223Phe_Tyr359Ala variant shed light on the impact of particular catalytic steps for the overall enantioselectivity of the reaction. In each case, intermediates and transition states from phenylacetate (PA) ligated Fe^{IV}=O centers up to the final products were analyzed, whereby the ideal initial *pro*-(*S*) and *pro*-(*R*) geometries, which had been geometrically optimized by DFT calculations (Figure S3–S5), were the starting points of all simulations. The complexes generally showed two distinct localizations of the phenyl rings on the intermediates that were prototypical for either the *pro*-(*S*) or the *pro*-(*R*) pathway (Figure 3b and Figure S6–S13). Inspection of the ligand geometries and energies in the *Sc*HMS WT protein suggested that product chirality was determined by the final hydroxylation step. The pro-(*S*) mechanism, to which the ligand is predisposed by preceding catalytic steps,[7,10d] resulted in a PA radical that displayed considerable out-of-plane flexibility. It oscillated between a *pro*-(*S*) (43%) and a *pro*-(*R*) (57%) conformation, thus apparently making both hydroxylation pathways equally feasible (Figure S10 and Table S4). The *pro*-(*S*) rebound transition state was then kinetically favored compared to the (*R*)-selective pathway. By contrast, during MD simulations of the newly designed (*R*)-MA synthase the first, high-valent Fe^{IV}=O complex of both *pro*-(*R*) and *pro*-(*S*) starting geometries adopted the *pro*-(*R*) conformation. The subsequent PA radicals were entrapped in their respective *pro*-(*S*) (99%) and *pro*-(*R*) positions (97%) (Figure S10), while the *pro*-(*S*) pathway was kinetically favored during hydroxylation. This suggests that the primary Fe^{IV}=O complex geometry co-determines enantioselectivity in the variant and apparently compensates for the kinetically favored (*S*)-trajectory during hydroxylation (Table S4). Overall, our computational method rationalized the experimentally observed enantioselectivities of the two enantio-complementary enzymes.

In summary, we demonstrated for the first time how the interplay of metal-center geometry and protein structure control enantioselective hydroxylation in a metalloenzyme. The consideration of this principle has allowed for the design of a highly (*R*)-selective MA synthase from an enantio-complementary HMS through the in vitro construction of a total of only ten enzyme variants. The resulting approximately 9300-fold enantioselectivity switch, the most pronounced change ever reported for an oxygenation, is accompanied by a threefold improvement of enzyme efficiency. The designed hydroxylase, which has no natural precedent, may open up a new route for efficient, sustainable (*R*)-MA biosynthesis from readily available renewable feedstocks. This work and its underlying principles may, furthermore, be

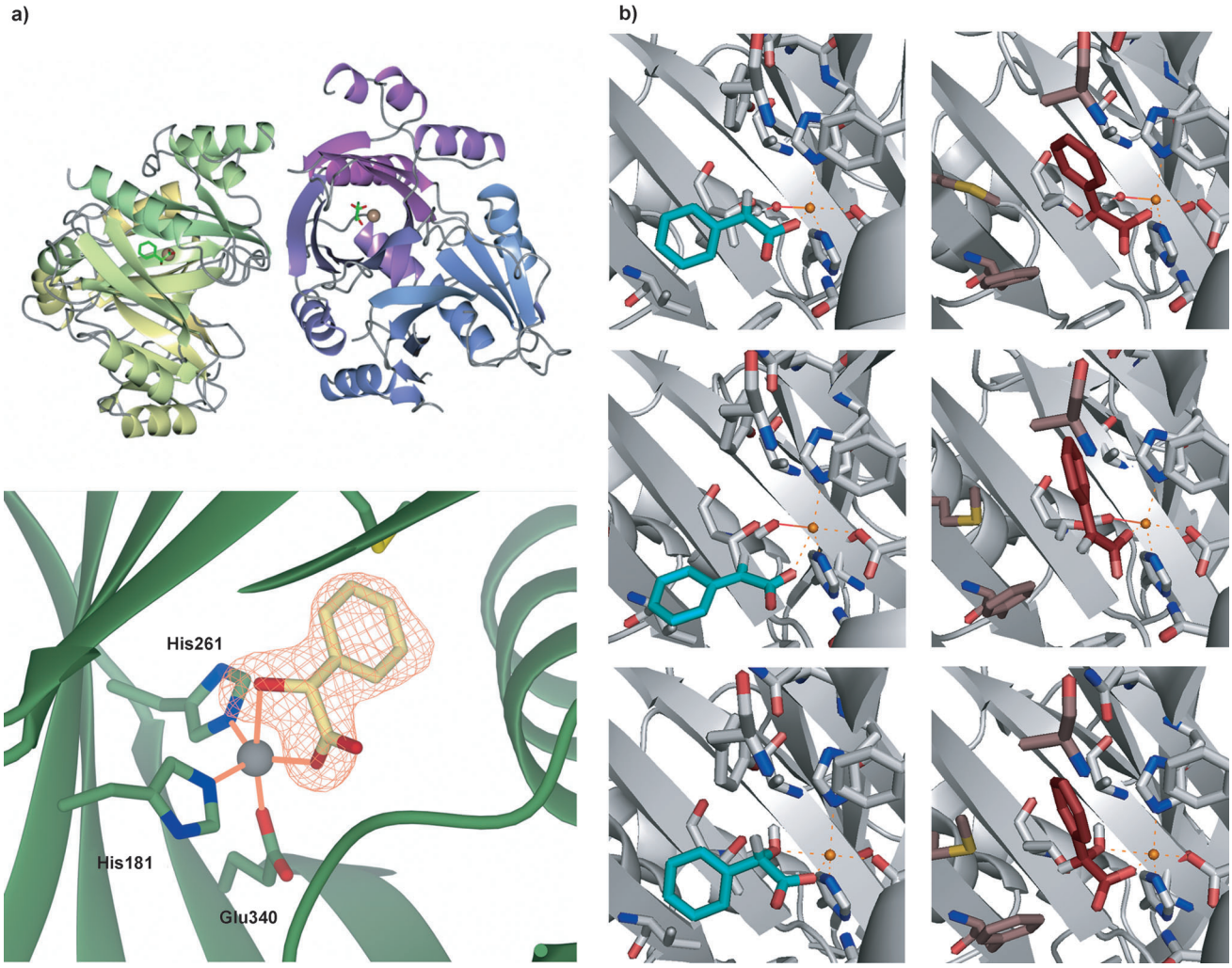

Figure 3. Interplay of protein structure and ligand orientation in the *Sc*HMS WT and the Ser221Met_Val223Phe_Tyr359Ala variant. a) Crystal structure of the (*R*)-selective *Sc*HMS triple variant. Top: overall structure of the observed dimer in complex with cobalt (brown) and the reaction product (*R*)-MA (green). Bottom: close-up of the active site. The coordinating oxygen atoms of (*R*)-MA (yellow) and the side chains of His261, His181, and Glu340 form a trigonal bipyramidal geometry around the cobalt atom (gray). The electron density of the ligand (coral) corresponds to the omit map (F_o-F_c map) contoured at a level of 3 σ obtained after the final rounds of refinement in the absence of the ligand. b) A structural representation of the catalytic steps that lead to chiral hydroxylation in WT *Sc*HMS (left) and in the (*R*)-selective triple mutant (right). The average structures of 10 ns MD simulations are shown, except in the lower right panel, which depicts the crystal structure of the mutant solved in this study. (Note that MD simulations gave similar active site geometries). The transition state of H-abstraction from PA by the Fe^{IV}=O center (upper row) results in an iron-bound hydroxy group and a substrate radical (middle row). The subsequent rebound step yields the chiral products (lower row). Residues within 5 Å of the metal (orange) are displayed—Ile335, Leu358, and Ile236 are omitted for clarity. Ligands of the (*S*)- and (*R*)-selective pathways are in teal and dark red, respectively. Mutations in the triple variant are shown in brown.

a first step in making enzymatic MNH Fe^{II} centers accessible as a resource for tailor-made biosynthetic oxygenations.

Received: May 29, 2013
Revised: July 1, 2013
Published online: July 23, 2013

Keywords: asymmetric catalysis · hydroxylation · metalloenzymes · non-heme iron · protein design

[1] K. Sanderson, *Nature* **2011**, *469*, 18–20.
[2] a) S. Kille, F. E. Zilly, J. P. Acevedo, M. T. Reetz, *Nat. Chem.* **2011**, *3*, 738–743; b) R. Agudo, G. D. Roiban, M. T. Reetz, *ChemBioChem* **2012**, *13*, 1465–1473; c) W. L. Tang, Z. Li, H. Zhao, *Chem. Commun.* **2010**, *46*, 5461–5463; d) S. Q. Pham, G. Pompidor, J. Liu, X. D. Li, Z. Li, *Chem. Commun.* **2012**, *48*, 4618–4620.
[3] V. B. Urlacher, M. Girhard, *Trends Biotechnol.* **2012**, *30*, 26–36.
[4] E. G. Kovaleva, J. D. Lipscomb, *Nat. Chem. Biol.* **2008**, *4*, 186–193.
[5] B. K. Hubbard, M. G. Thomas, C. T. Walsh, *Chem. Biol.* **2000**, *7*, 931–942.
[6] O. W. Choroba, D. H. Williams, J. B. Spencer, *J. Am. Chem. Soc.* **2000**, *122*, 5389–5390.
[7] C. M. L. Di Giuro, C. Konstantinovics, U. Rinner, C. Nowikow, E. Leitner, G. D. Straganz, *PLoS One* **2013**, DOI: 10.1371/journal.pone.0068932.
[8] D. D. Shah, J. A. Conrad, B. Heinz, J. M. Brownlee, G. R. Moran, *Biochemistry* **2011**, *50*, 7694–7704.

[9] J. Brownlee, P. He, G. R. Moran, D. H. Harrison, *Biochemistry* **2008**, *47*, 2002 – 2013.
[10] M. L. Neidig, A. Decker, O. W. Choroba, F. Huang, M. Kavana, G. R. Moran, J. B. Spencer, E. I. Solomon, *Proc. Natl. Acad. Sci. USA* **2006**, *103*, 12966 – 12973; b) S. P. de Visser, *Angew. Chem.*, **2006**, *118*, 1822 – 1825; *Angew. Chem. Int. Ed.*, **2006**, 45, 1790 – 1793; c) S. Sinnecker, N. Svensen, E. W. Barr, S. Ye, J. M. Bollinger, Jr., F. Neese, C. Krebs, *J. Am. Chem. Soc.* **2007**, 129, 6168 – 6179; d) A. Wojcik, E. Broclawik, P. E. Siegbahn, T. Borowski, *Biochemistry* **2012**, 51, 9570-9580.
[11] T. K. Paine, H. Zheng, L. Que Jr. , *Inorg. Chem.* **2005**, *44*, 474 – 476.
[12] a) M. Gunsior, J. Ravel, G. L. Challis, C. A. Townsend, *Biochemistry* **2004**, *43*, 663 – 674; b) J. M. Brownlee, B. Heinz, J. Bates, G. R. Moran, *Biochemistry* **2010**, *49*, 7218 – 7226.

